

## Evolution of charge density waves from three-dimensional to quasi-two-dimensional in kagome superconductors $\text{Cs}(\text{V}_{1-x}\text{M}_x)_3\text{Sb}_5$ ( $M = \text{Nb}, \text{Ta}$ )

Qian Xiao <sup>1,\*</sup>, Qizhi Li,<sup>1,\*</sup> Jinjin Liu,<sup>2,3,\*</sup> Yongkai Li,<sup>2,3,4</sup> Wei Xia,<sup>5,6</sup> Xiquan Zheng,<sup>1</sup>  
Yanfeng Guo,<sup>5,6</sup> Zhiwei Wang,<sup>2,3,4,†</sup> and Yingying Peng <sup>1,7,‡</sup>

<sup>1</sup>International Center for Quantum Materials, School of Physics, Peking University, Beijing 100871, China

<sup>2</sup>Centre for Quantum Physics, Key Laboratory of Advanced Optoelectronic Quantum Architecture and Measurement (MOE),  
School of Physics, Beijing Institute of Technology, Beijing 100081, China

<sup>3</sup>Beijing Key Lab of Nanophotonics and Ultrafine Optoelectronic Systems, Beijing Institute of Technology, Beijing 100081, China

<sup>4</sup>Material Science Center, Yangtze Delta Region Academy of Beijing Institute of Technology, Jiaxing 314011, China

<sup>5</sup>School of Physical Science and Technology, ShanghaiTech University, Shanghai 201210, China

<sup>6</sup>ShanghaiTech Laboratory for Topological Physics, ShanghaiTech University, Shanghai 201210, China

<sup>7</sup>Collaborative Innovation Center of Quantum Matter, Beijing 100871, China



(Received 4 April 2023; revised 8 June 2023; accepted 20 June 2023; published 5 July 2023)

The kagome material  $\text{AV}_3\text{Sb}_5$  ( $A = \text{K}, \text{Rb}, \text{Cs}$ ) with geometry frustration hosts nontrivial topological electronic structures, electronic nematicity, the charge density wave (CDW), and superconductivity, providing an ideal platform to study the interplay between these phases. Specifically, in pressurized or substituted  $\text{CsV}_3\text{Sb}_5$ , the relationship between CDW and superconductivity is unusual and remains to be fully understood. Recently, coexisting and competing  $2 \times 2 \times 4$  and  $2 \times 2 \times 2$  CDW phases were discovered in  $\text{CsV}_3\text{Sb}_5$ . To investigate the evolution of the CDW phases with the substitution of V atoms, we performed x-ray diffraction experiments on  $\text{Cs}(\text{V}_{1-x}\text{Ta}_x)_3\text{Sb}_5$  and  $\text{Cs}(\text{V}_{1-x}\text{Nb}_x)_3\text{Sb}_5$ . Our results indicate that in all substituted samples, the discrete CDW reflection points in pristine  $\text{CsV}_3\text{Sb}_5$  change to rodlike structures along the  $c^*$  direction. This suggests that the long-ranged three-dimensional CDW becomes quasi-two-dimensional by the substitution of V by Ta/Nb. Moreover, our temperature-dependent measurements show that there is no hysteresis behavior of CDW signals, indicating that even a slight substitution of Nb or Ta as low as 0.021 and 0.04, respectively, can easily suppress the  $2 \times 2 \times 4$  CDW phase. These findings uncover the CDW evolution upon substitution of V atoms in  $\text{CsV}_3\text{Sb}_5$ , providing insights into the microscopic mechanism of CDW and helping to understand the interplay between intertwined phases and superconductivity.

DOI: [10.1103/PhysRevMaterials.7.074801](https://doi.org/10.1103/PhysRevMaterials.7.074801)

### I. INTRODUCTION

The kagome nets, composed of three interwoven triangular lattices, are geometrically frustrated and have been predicted to possess flat bands, Dirac cones, and van Hove singularities (vHSs) in theory, offering an opportunity for the realization of novel topological quantum states such as the quantum spin liquid [1–3]. At van Hove filling, a diverse phase diagram emerges with various electronic instabilities such as spin and charge bond orders, superconductivity, and the charge density wave (CDW), all of which can be controlled by Hubbard interactions  $U$  [4–6]. The kagome family  $\text{AV}_3\text{Sb}_5$  ( $A = \text{K}, \text{Rb}, \text{Cs}$ ) has been identified as a topological metal with a superconducting transition occurring below 3 K, leading to a surge in research in condensed matter physics [7–9], and numerous exotic physical properties of this family were revealed. A CDW transition occurs between 78 K and 103 K [7–10], and the abnormal Hall effect (AHE) emerges simultaneously, reaching a magnitude of  $10\,000 \Omega^{-1} \text{cm}^{-1}$  at low tempera-

ture without any detected local spin moments [11–13]. By substituting V sites, AHE decreases with decreasing CDW, indicating a strong correlation between CDW and AHE [14,15]. Moreover, a twofold rotation symmetry is observed in the CDW state [16–18] and persists into the superconducting phase in  $\text{CsV}_3\text{Sb}_5$  [19]. Electronic nematicity develops below the CDW transition temperature  $T_{\text{CDW}}$ , which undergoes a nematic transition at around 35 K [20]. Muon spin relaxation measurements suggest the concurrence of the time-reversal-symmetry breaking and CDW phase formation [17,21]. Thus, investigating the CDW phases is crucial for comprehending these exotic properties in  $\text{AV}_3\text{Sb}_5$ .

$\text{CsV}_3\text{Sb}_5$  exhibits a rich array of exotic properties, including coexisting and competing  $2 \times 2 \times 4$  and  $2 \times 2 \times 2$  CDW phases at low temperature, which have been demonstrated by combining x-ray scattering experiments with density-functional theory calculations [22]. It is therefore important to investigate how external stimuli such as pressure and substitution may affect the CDW phase and other properties, especially superconductivity. Previous studies on pressurized and Sn-doped  $\text{CsV}_3\text{Sb}_5$  reveal an unusual competition between CDW and superconductivity, where superconducting transition temperature  $T_c$  shows double peaks with the suppression of CDW phases [23–25]. This unique behavior in

\*These authors contributed equally to this work.

†zhiweiwang@bit.edu.cn

‡yingying.peng@pku.edu.cn

$\text{CsV}_3\text{Sb}_5$  differs from that of other  $\text{AV}_3\text{Sb}_5$  family members [26,27]. Notably, substituting V sites has been shown to have a distinct effect from doping Sb sites in  $\text{CsV}_3\text{Sb}_5$ . Doping Sb with Sn resulted in the observation of prominent double  $T_c$  domes [25], while  $T_c$  entered a plateau after the initial enhancement in  $\text{Cs}(\text{V}_{1-x}\text{Ta}_x)_3\text{Sb}_5$  [28]. From an electronic structure perspective, holes are introduced in  $\text{CsV}_3\text{Sb}_{5-x}\text{Sn}_x$ , which lifts the Sb-derived electron-like band at the  $\Gamma$  point up and above Fermi level, but only causes a relatively small change in the V-derived vHS at the  $M$  point [25]. In contrast, the isovalent substitution of V by Nb lifts the saddle point up away from the Fermi level and shifts the electron-like band at the  $\Gamma$  point downward [15,29]. Previous x-ray diffraction (XRD) studies on  $\text{CsV}_3\text{Sb}_{5-x}\text{Sn}_x$  found that the interlayer CDW correlations become short-ranged upon doping Sb by Sn, with Sn mainly occupying the Sb sites in the kagome plane [25,30]. However, XRD study on  $\text{CsV}_3\text{Sb}_5$ -derived kagome materials with V substitution is still lacking. The CDW phase, which is accompanied by the deformation of the vanadium kagome net, is believed to arise from the scattering between vHSs at the  $M$  point [10,15,29,31]. However, it has also been proposed that electron-phonon coupling plays a crucial role in the formation of the CDW phase [32–34]. Therefore, it is interesting to study the effect of substituting V sites on the CDW phase.

Here we employ x-ray diffraction to investigate the evolution of CDW phases by substituting V with Ta and Nb in  $\text{CsV}_3\text{Sb}_5$ . As substitution levels increase, the CDW transition temperature decreases smoothly, while the enhancement of the superconducting transition temperature is nonmonotonic. Compared to pristine  $\text{CsV}_3\text{Sb}_5$ , the XRD patterns of Nb and Ta substituted  $\text{CsV}_3\text{Sb}_5$  show rodlike CDW signals along the  $c^*$  direction, indicating that CDW correlations along the  $c$  direction are rapidly suppressed by a slight substitution. The estimated correlation length along the out-of-plane direction is only  $\sim 2c$  in  $\text{Cs}(\text{V}_{1-x}\text{Ta}_x)_3\text{Sb}_5$  ( $x = 0.067$ ). Our temperature-dependent XRD measurements on substituted  $\text{CsV}_3\text{Sb}_5$  samples demonstrate a complete suppression of the  $2 \times 2 \times 4$  CDW phase, evidenced by the disappearance of the hysteresis behavior of CDW signals. Furthermore, the CDW transition width broadens with increasing substitution levels. These findings shed light on understanding the microscopic mechanism of CDW and the interplay between the intertwined phases in the kagome superconductor  $\text{CsV}_3\text{Sb}_5$ .

## II. MATERIALS AND METHODS

We have studied three substitution levels of  $\text{Cs}(\text{V}_{1-x}\text{Ta}_x)_3\text{Sb}_5$ :  $x = 0.04$ , 0.067, and 0.1, and four substitution levels of  $\text{Cs}(\text{V}_{1-x}\text{Nb}_x)_3\text{Sb}_5$ :  $x = 0.021$ , 0.023, 0.026, and 0.068. The crystalline  $\text{CsV}_3\text{Sb}_5$ ,  $\text{Cs}(\text{V}_{1-x}\text{Ta}_x)_3\text{Sb}_5$ , and  $\text{Cs}(\text{V}_{1-x}\text{Nb}_x)_3\text{Sb}_5$  samples in the present XRD study were grown by a self-flux growth method [22,28]. Chemical composition was identified on a JEOL scanning electron microscope (JSM-7500F) equipped with energy dispersive x-ray spectroscopy. The doping concentration was determined by averaging measurements from 10 different positions on each crystal with an uncertainty of 1%. Electronic transport measurements with temperatures down to 1.8 K were carried out on a physical property measurement system (Quantum

Design). The contacts were prepared by using gold wires which were attached by room-temperature-cured silver paste to the sample.

We used a custom-designed x-ray instrument equipped with a Xenocs Genix3D Mo  $K_\alpha$  (17.48 keV) x-ray source to perform single-crystal x-ray diffraction measurements. The instrument provided a beam spot size of 150  $\mu\text{m}$  at the sample position and  $\sim 2.5 \times 10^7$  photons/sec. We also performed high-resolution XRD measurements on pristine  $\text{CsV}_3\text{Sb}_5$  and Ta-substituted  $\text{CsV}_3\text{Sb}_5$  single crystals using a highly monochromatic Cu  $K_{\alpha 1}$  (8.048 keV) radiation x-ray source with  $\sim 4 \times 10^6$  photons/sec [22]. The samples were mounted on a 4-circle Huber diffractometer and cooled by a closed-cycle cryostat with a temperature accuracy of about  $\pm 91$  mK and temperature stability of about  $\pm 30$  mK. One beryllium (Be) dome served as a vacuum and radiation shield to cool the sample down to 18 K. We collected scattering signals using a highly sensitive single-photon counting PILATUS3 R 1M solid state area detector with  $980 \times 1042$  pixels, each pixel size being 172  $\mu\text{m} \times 172 \mu\text{m}$ . To map the 3-dimensional momentum space, we took images in  $0.1^\circ$  increments while rotating the samples [22].

We indexed the x-ray diffraction pattern of  $\text{Cs}(\text{V}_{1-x}\text{M}_x)_3\text{Sb}_5$  ( $M = \text{Nb}, \text{Ta}$ ) using a hexagonal unit cell based on the main Bragg peaks [22]. In pristine  $\text{CsV}_3\text{Sb}_5$ , the lattice parameters are  $a = b \simeq 5.53$   $\text{\AA}$  and  $c \simeq 9.28$   $\text{\AA}$ . While the  $c$  lattice parameter remains almost unchanged in the Nb/Ta substituted  $\text{CsV}_3\text{Sb}_5$ , the in-plane lattice parameter

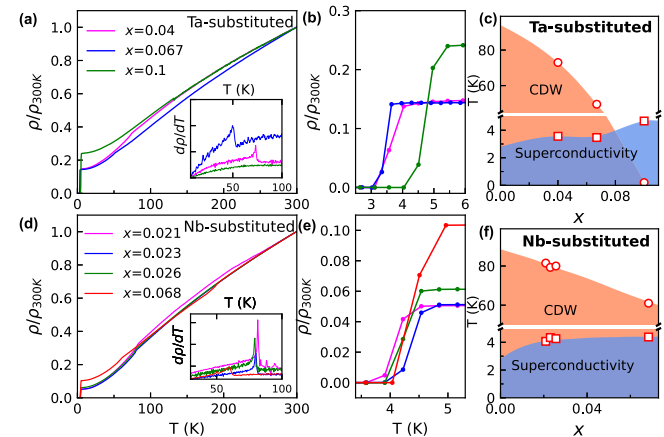


FIG. 1. [(a),(d)] Temperature dependence of in-plane resistivity measured from 1.8 K to 300 K for  $\text{Cs}(\text{V}_{1-x}\text{Ta}_x)_3\text{Sb}_5$  and  $\text{Cs}(\text{V}_{1-x}\text{Nb}_x)_3\text{Sb}_5$ , respectively. The data were normalized to the resistivity at 300 K; the inset shows  $d\rho/dT$  as a function of temperature near the CDW transition. The  $d\rho/dT$  curve of  $\text{Cs}(\text{V}_{1-x}\text{Ta}_x)_3\text{Sb}_5$  ( $x = 0.067$ ) was obtained by deriving the smoothed  $R$ - $T$  curve to reduce the noise level. [(b),(e)] Zoomed-in views of the  $\rho(T)$  curves near the superconductivity transition temperatures for  $\text{Cs}(\text{V}_{1-x}\text{Ta}_x)_3\text{Sb}_5$  and  $\text{Cs}(\text{V}_{1-x}\text{Nb}_x)_3\text{Sb}_5$ , respectively. The schematic phase diagrams of  $\text{Cs}(\text{V}_{1-x}\text{Ta}_x)_3\text{Sb}_5$  and  $\text{Cs}(\text{V}_{1-x}\text{Nb}_x)_3\text{Sb}_5$  are shown in (c) and (f), respectively. The CDW transition temperatures determined from the peak of the  $d\rho/dT$  curve are indicated by circles in (c) and (f). The superconducting transition temperatures determined by the midpoint of the resistivity drop are represented by squares.

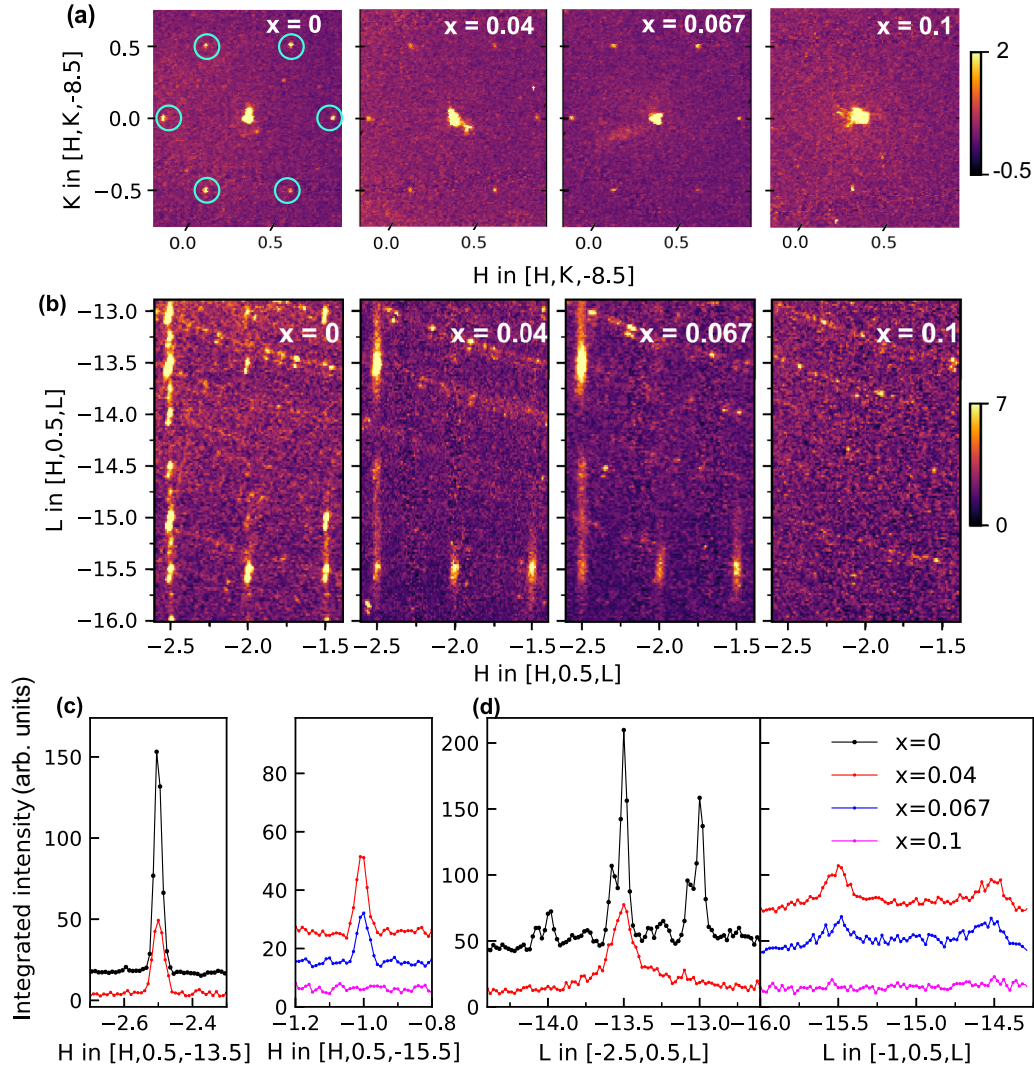


FIG. 2. XRD measurements for  $\text{Cs}(\text{V}_{1-x}\text{Ta}_x)_3\text{Sb}_5$  with four different Ta substitution levels taken at 18 K using a Mo  $K_\alpha$  x-ray source. (a)  $(H, K)$  maps of reciprocal space at  $L = -8.5$ . (b)  $(H, L)$  maps of reciprocal space at  $K = 0.5$ . The cyan circles indicate the CDW diffraction points. (c)  $H$  cuts of  $[-2.5, 0.5, -13.5]$  and  $[-1, 0.5, -15.5]$  are shown in the left and right panels, respectively. (d)  $L$  cuts of  $[-2.5, 0.5, L]$  and  $[-1, 0.5, L]$  are shown in the left and right panels, respectively. An offset is added for clarity. The double peaks of  $x = 0$  originate from the small nonmonochromatic x-ray source. The arc signals in color maps come from beryllium domes.

$a$  ( $= b$ ) becomes larger by substituting V with Ta, which increases to  $5.57 \text{ \AA}$  for  $\text{Cs}(\text{V}_{1-x}\text{Ta}_x)_3\text{Sb}_5$  ( $x = 0.1$ ). We did not observe any discernible change in the lattice parameters for Nb-doped samples compared to the pristine samples. Throughout this paper, we label the Miller indices  $(H, K, L)$  according to the undistorted high-temperature phase (see details of indexation in Ref. [22]).

### III. RESULTS

#### A. Resistivity measurements

Figure 1 shows the resistivity measurements of our  $\text{Cs}(\text{V}_{1-x}\text{M}_x)_3\text{Sb}_5$  ( $M = \text{Nb}, \text{Ta}$ ) single crystals. The presence of a kink in the resistivity versus temperature curve, particularly emphasized in the  $d\rho/dT$  curve [Figs. 1(a) and 1(d)], signifies the occurrence of the CDW phase transition. Based on these observations, we have determined the  $T_{\text{CDW}}$  values to be 94 K for the pristine sample, 73 K for the  $x = 0.04$

Ta-substituted sample, and 49.5 K for the  $x = 0.067$  Ta-substituted sample. Notably, no CDW transition was observed in the  $x = 0.1$  sample. In the case of Nb-substituted samples,  $T_{\text{CDW}}$  was determined to be 81.5 K, 80 K, 79.3 K, and 61 K for the  $x = 0.021, 0.023, 0.026,$  and  $0.068$  samples, respectively. The substitution of Ta and Nb for V resulted in the suppression of CDW, leading to a decrease in the CDW transition temperature and reduced sharpness of the peak at  $T_{\text{CDW}}$  in the  $d\rho/dT$  curve. However, the superconducting transition temperature  $T_c$  shows a nonmonotonic increase with substitution [Figs. 1(b) and 1(e)]. For Ta-substituted  $\text{CsV}_3\text{Sb}_5$ ,  $T_c$ , determined by the midpoint of the resistivity drop, is enhanced from 2.8 K in the pristine sample to 3.5 K in  $x = 0.04$ , and then remains almost the same until  $x = 0.067$ . At  $x = 0.1$ , where the CDW phase is completely suppressed,  $T_c$  increases to 4.7 K [Fig. 1(b)]. Notably, previous studies have reported that the superconducting volume fraction in  $\text{Cs}(\text{V}_{1-x}\text{Ta}_x)_3\text{Sb}_5$  remains close to 1, even at the highest Ta-substitution level

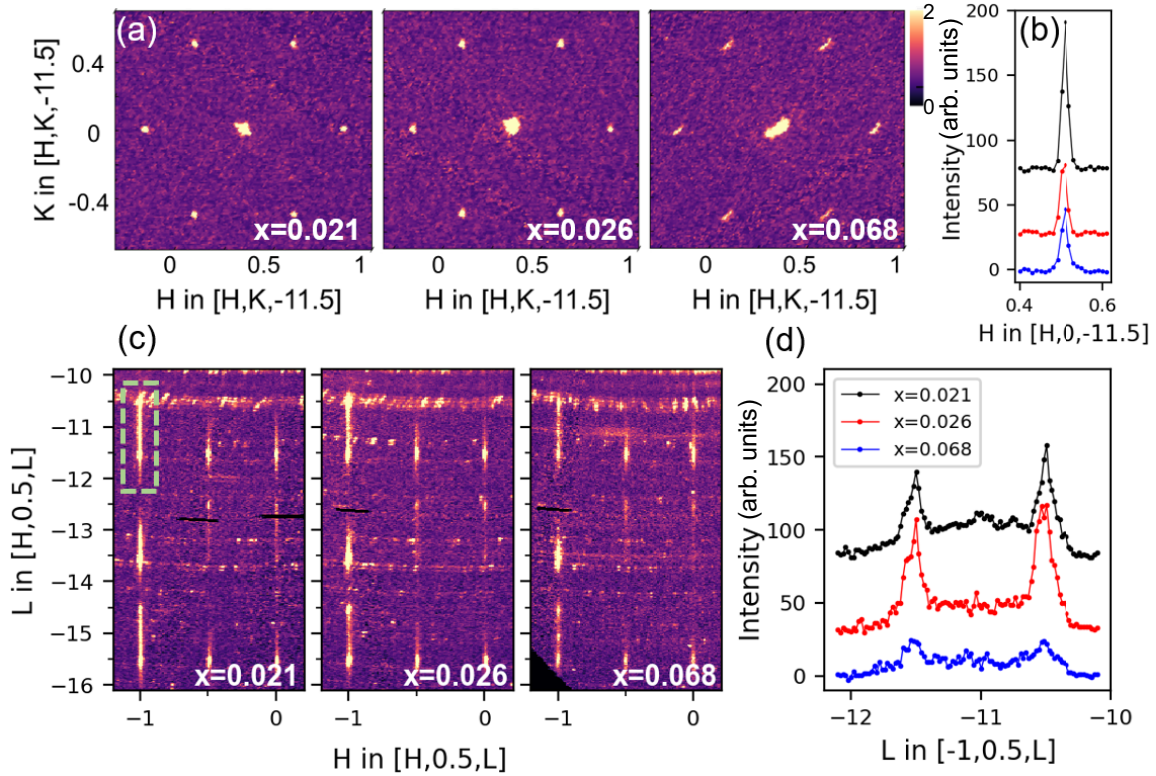


FIG. 3. (a) The  $(H, K)$  maps of reciprocal space at  $L = -11.5$  for  $\text{Cs}(\text{V}_{1-x}\text{Nb}_x)_3\text{Sb}_5$  with three different Nb substitution levels measured at 18 K using a Mo  $K_\alpha$  x-ray source. (b)  $H$  cuts of  $[H, 0, -11.5]$  at 18 K. Offset is added for clarity. (c)  $(H, L)$  maps of reciprocal space at  $K = 0.5$ . (d)  $L$  cuts of  $[-1, 0.5, L]$  at 18 K. Offset is added for clarity. The arc signals in color maps come from beryllium domes.

of  $x = 0.14$ , indicating that doping has little effect on the superconducting volume fraction [35,36]. In Nb-substituted  $\text{CsV}_3\text{Sb}_5$ ,  $T_{\text{CDW}}$  is suppressed from 94 K to 70 K with Nb substitution increasing to 0.068, while  $T_c$  is enhanced from 2.8 K in the pristine sample to  $\sim 4$  K and then remains almost the same in the substitution range from 0.021 to 0.068, as shown in Figs. 1(d) and 1(e). The schematic phase diagrams for  $\text{Cs}(\text{V}_{1-x}\text{Ta}_x)_3\text{Sb}_5$  and  $\text{Cs}(\text{V}_{1-x}\text{Nb}_x)_3\text{Sb}_5$  obtained from resistivity measurement results are shown in Figs. 1(c) and 1(f), respectively. However, the study of Nb substitution persists only up to  $x \simeq 0.07$  due to the solubility limit, where the CDW is not fully suppressed [15].

### B. XRD measurements of CDWs at low temperature

In order to investigate the effects of substitution on the CDWs in  $\text{Cs}(\text{V}_{1-x}\text{Ta}_x)_3\text{Sb}_5$  and  $\text{Cs}(\text{V}_{1-x}\text{Nb}_x)_3\text{Sb}_5$ , we conducted XRD measurements with different substitution levels. The samples were cooled from room temperature to 18 K at a rate of 2 K/min, and Mo  $K_\alpha$  radiation was used as the x-ray source. Figure 2(a) shows the evolution of the  $(H, K)$  map at  $L = -8.5$  for  $\text{Cs}(\text{V}_{1-x}\text{Ta}_x)_3\text{Sb}_5$ . As V is substituted by Ta, the CDW diffraction points are weakened and eventually disappear at  $x = 0.1$ . The changes in the CDW are more pronounced along the  $L$  direction as shown in Fig. 2(b). In the  $(H, L)$  map at  $K = 0.5$ , the discrete CDW diffraction points with integer, half-integer, and quarter-integer  $L$  values in pristine  $\text{CsV}_3\text{Sb}_5$  become rodlike and are centered at half-integer  $L$  in the substituted samples. This suggests that the CDW

becomes quasi-two-dimensional (quasi-2D) as V is substituted by Ta. To better visualize the change of CDW peaks along in-plane and out-of-plane directions, we compared the  $H$  and  $L$  cuts at different substitution levels, as shown in Figs. 2(c) and 2(d). It is observed that the widths of the CDW peaks have broadened in both the in-plane and out-of-plane directions, as compared to the pristine sample. Although the diffraction peaks stemming from the  $2 \times 2 \times 4$  CDW at quarter-integer  $L$  values may be obscured by the broad tail of the CDW peak centered at half-integer  $L$ , our temperature-dependent XRD measurements, as discussed later, revealed the absence of the expected hysteresis behavior associated with the  $2 \times 2 \times 4$  CDW phase [22]. This finding confirms the disappearance of the  $2 \times 2 \times 4$  CDW phase in the substituted samples. Figure 3 shows the XRD measurements for  $\text{Cs}(\text{V}_{1-x}\text{Nb}_x)_3\text{Sb}_5$  crystals. Similar to Ta substitution, the CDW diffraction signals of Nb-substituted  $\text{CsV}_3\text{Sb}_5$  also become rodlike in the  $(H, L)$  map at  $K = 0.5$ , indicating a short-ranged correlation along the  $L$  direction. These results suggest that substituting V with Ta/Nb hinders the establishment of long-ranged three-dimensional (3D) CDW correlations.

To quantitatively reveal the correlation lengths with substitution, we performed high-resolution XRD measurements on pristine  $\text{CsV}_3\text{Sb}_5$  and  $\text{Cs}(\text{V}_{1-x}\text{Ta}_x)_3\text{Sb}_5$  ( $x = 0.067$ ) single crystals using a highly monochromatic Cu  $K_{\alpha 1}$  (8.048 keV) radiation x-ray source at 18 K. The upper panel and lower panel of Fig. 4 show the results for the pristine and substituted samples, respectively. We fitted the CDW profiles along both in-plane and out-of-plane directions using

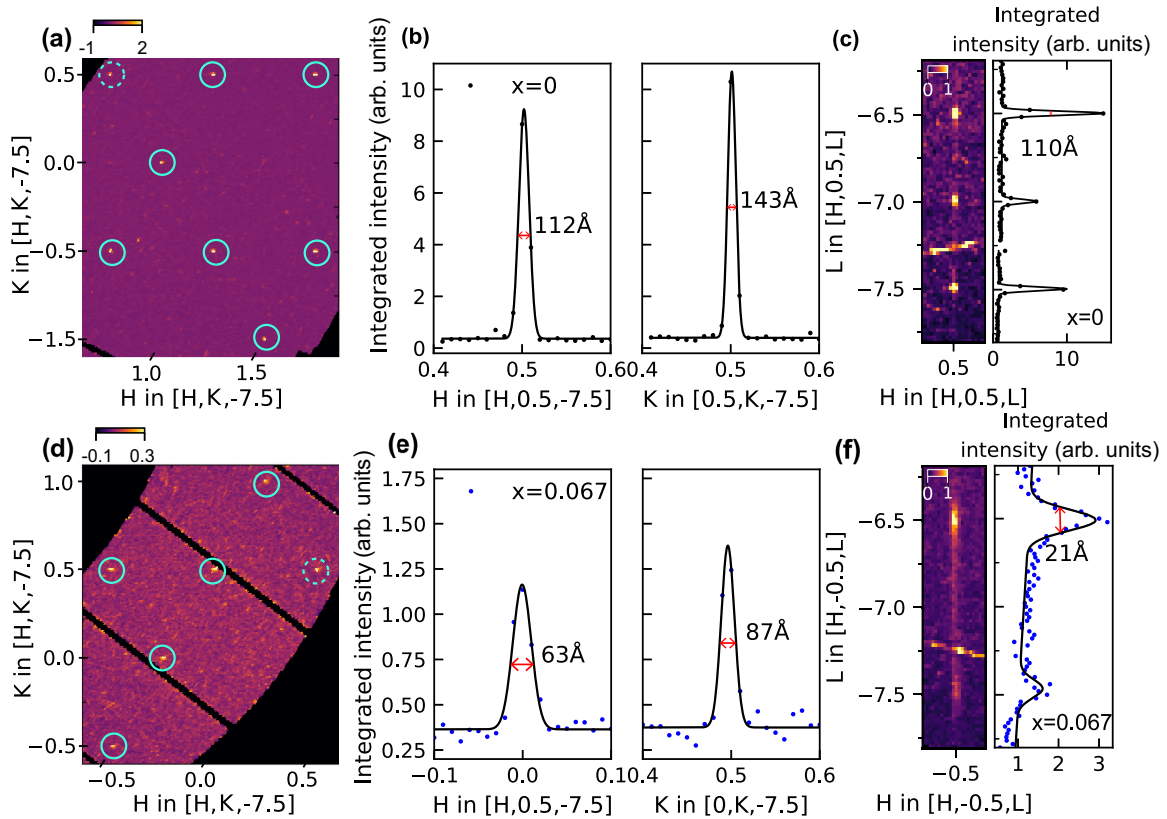


FIG. 4. XRD measurements collected at 18 K using a highly monochromatic Cu  $K_{\alpha 1}$  (8.048 keV) radiation x-ray source for  $\text{Cs}(\text{V}_{1-x}\text{Ta}_x)_3\text{Sb}_5$ . (a), (d)  $(H, K)$  maps of reciprocal space at  $L = -7.5$  for the pristine sample and  $x = 0.067$ , respectively. The cyan circles indicate the CDW diffraction points. The  $H$  and  $K$  cuts of CDW diffraction peaks highlighted by the dashed cyan circle in (a) and (d) are shown in (b) and (e), respectively. [(c),(f)]  $(H, L)$  maps of reciprocal space for the pristine sample at  $K = 0.5$  and  $x = 0.067$  at  $K = -0.5$ , respectively. The corresponding  $L$  cut is shown in the right panel. Solid black lines are fits with Gaussian functions and a linear background. The correlation length, defined as  $1/\text{HWHM}$ , is shown in the figure.

Gaussian functions and extracted the correlation length  $\xi$ , defined as  $1/\text{HWHM}$  (half width at half maximum). The in-plane correlation lengths along the  $H$  and  $K$  directions reduced from  $\sim 112$  Å and  $\sim 143$  Å in the pristine sample to  $\sim 63$  Å and  $\sim 87$  Å in the  $x = 0.067$  sample [see Figs. 4(b) and 4(e) for comparison]. It is worth noting that the correlation lengths in the pristine samples are limited by resolution, whereas this is not the case for the substituted samples. As a result, further investigations are required to explore the doping evolution of correlation length and its correlation with the superconducting transition temperature. We notice that the in-plane CDW reflections are anisotropic, as the correlation length along the  $K$  direction is longer than the  $H$  direction in both pristine and substituted samples. The estimated anisotropy, defined as  $(\xi_K - \xi_H)/(\xi_K + \xi_H)$ , increases from 12% in the pristine sample to 16% in the  $x = 0.067$  sample. Whether this anisotropy may relate to electron nematicity needs further investigation. Intriguingly, the correlation length along the  $L$  direction significantly reduces from  $\sim 110$  Å in the pristine sample to  $\sim 21$  Å in  $\text{Cs}(\text{V}_{1-x}\text{Ta}_x)_3\text{Sb}_5$  ( $x = 0.067$ ), indicating that only the neighboring interlayers are correlated.

### C. Temperature evolution of CDW in substituted samples

To investigate the temperature evolution of the CDW phase in Ta- and Nb-substituted  $\text{CsV}_3\text{Sb}_5$  samples, we conducted

temperature-dependent XRD measurements using a Mo  $K_{\alpha}$  radiation x-ray source. We cooled the samples from room temperature to 18 K at a rate of 2 K/min, then performed warming and cooling measurements. The resulting data for  $\text{Cs}(\text{V}_{1-x}\text{Ta}_x)_3\text{Sb}_5$  and  $\text{Cs}(\text{V}_{1-x}\text{Nb}_x)_3\text{Sb}_5$  are presented in Figs. 5 and 6, respectively. Each data point is the average of six repeated measurements at each temperature to improve statistical accuracy, which took about one hour per temperature. The normalized intensity was obtained by integrating the entire CDW rods and normalizing the low-temperature signal.

We observed no thermal hysteresis behavior in the CDW diffraction signals in any of our substituted  $\text{CsV}_3\text{Sb}_5$  samples. This is in sharp contrast to the pristine sample, where the  $2 \times 2 \times 4$  CDW undergoes a transition at 93 K in the warming process and 89 K in the cooling process, exhibiting a 4 K thermal hysteresis behavior [22]. The lack of thermal hysteresis behavior of CDW diffraction signals in  $\text{Cs}(\text{V}_{1-x}\text{M}_x)_3\text{Sb}_5$  ( $M = \text{Nb}, \text{Ta}$ ) indicates the destruction of the  $2 \times 2 \times 4$  CDW phase. In the pristine sample,  $T_{\text{CDW}}$  was 94 K, whereas the CDW peaks disappear above 76 K and 57.6 K in the samples with Ta substitutions of  $x = 0.04$  and 0.067, respectively. No CDW was observed in the  $x = 0.1$  Ta-substituted sample. In the case of Nb-substituted samples, the CDW peaks vanish above temperatures of 86.1 K, 85.6 K, 82.7 K, and 71.2 K for the  $x = 0.021, 0.023, 0.026,$  and  $0.068$  samples, respectively.

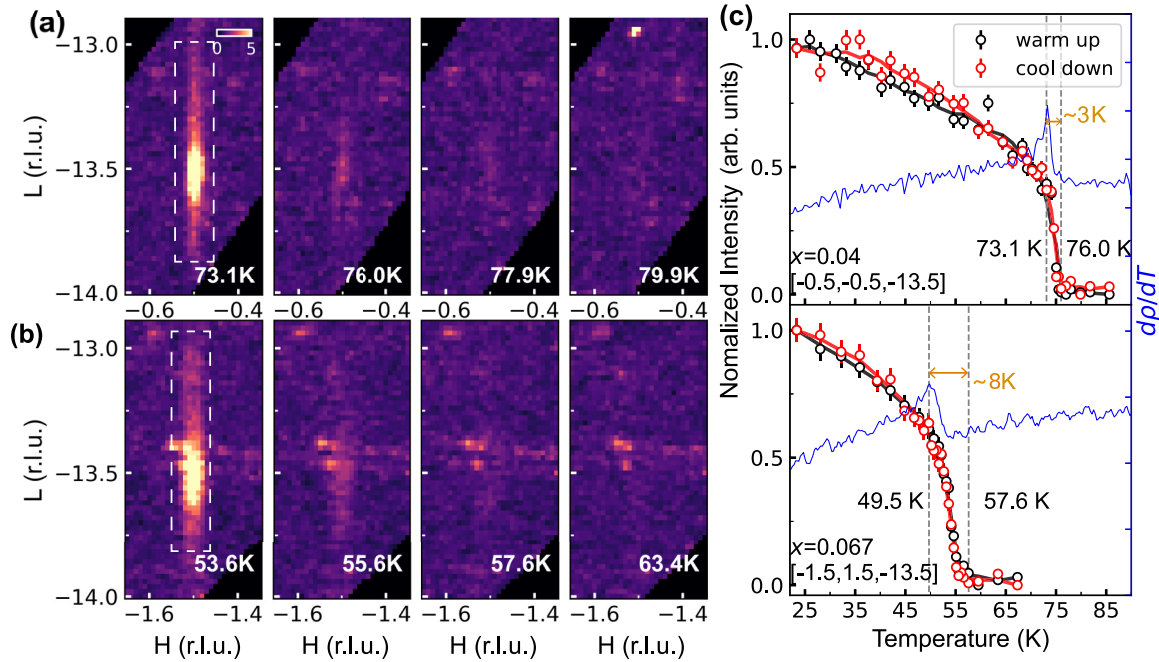


FIG. 5. Temperature dependence of the CDW in Ta-substituted samples. (a) The CDW profiles in  $x = 0.04$  measured at 73.1 K, 76 K, 77.9 K, and 79.9 K. (b) The CDW profiles in  $x = 0.067$  measured at 53.6 K, 55.6 K, 57.6 K, and 63.4 K. (c) Temperature dependence of CDW in two Ta-substituted samples. The temperature evolution curves overlap well during the warming and cooling processes. The  $d\rho/dT$  curve is also appended for comparison. The dashed lines indicate the onset decrease and disappearance of the CDW peak intensity. The transition width is indicated in the figure.

The estimated error bar for the CDW transition temperature is  $\pm 0.12$  K, considering the temperature accuracy and stability of our x-ray instrument [22].

We observe that the CDW transition temperature determined from resistivity data coincides with the onset decrease of the CDW peak intensity in the XRD measurements, as shown in Figs. 5(c) and 6(c). Furthermore, the CDW transition broadened with increasing substitution levels. The CDW transition in the pristine sample is very sharp, with a transition width within 2 K [22]. In contrast, the CDW transition width broadens to 8 K in the  $\text{Cs}(\text{V}_{1-x}\text{Ta}_x)_3\text{Sb}_5$  ( $x = 0.067$ ) sample and 10 K in the  $\text{Cs}(\text{V}_{1-x}\text{Nb}_x)_3\text{Sb}_5$  ( $x = 0.068$ ) sample. These results suggest that the substitution destroys the formation of long-ranged CDW orders.

#### IV. DISCUSSION

Our results indicate that the CDW phase of  $\text{Cs}(\text{V}_{1-x}\text{M}_x)_3\text{Sb}_5$  ( $M = \text{Nb}, \text{Ta}$ ) is suppressed not only by a decrease in the CDW transition temperature but also by a reduction in the CDW correlation lengths, particularly along the  $c$  direction. Specifically, the  $2 \times 2 \times 4$  CDW phase disappears with slight substitution and the remaining  $2 \times 2 \times 2$  CDW phase becomes quasi-2D with a correlation length of only about 21 Å, i.e., 2 unit cells along the  $c$  direction. In pristine  $\text{CsV}_3\text{Sb}_5$ , the CDW phases arise from interlayer stacking of layers with the same in-plane CDW modulation [17,20,22]. Although the phase shift between adjacent kagome layers persists in substituted samples, the random stacking along the  $c$  direction results in rodlike signals in the XRD pattern of the substituted samples. Similarly, the

rodlike signals in  $\text{Y}_5\text{Ru}_2\text{O}_{12}$  are suggested to originate from stacking faults [37].

Rodlike CDW signals have also been observed in Sn-doped  $\text{CsV}_3\text{Sb}_5$ , which are found centered at both half-integer and integer  $L$  values [30]. However, in our study, we find CDW diffraction peaks at integer  $L$  to be invisible, likely due to their weak intensities. Some CDW diffraction signals centered at half-integer  $L$  are asymmetric, leading us to speculate that the diffraction peaks at integer  $L$  are hidden in the broadened CDW reflection signals centered at half-integer  $L$ . Compared to Sn-doped  $\text{CsV}_3\text{Sb}_5$  [30], the CDW correlation lengths are shorter in both in-plane and out-of-plane directions in the substituted  $\text{Cs}(\text{V}_{1-x}\text{M}_x)_3\text{Sb}_5$  ( $M = \text{Nb}, \text{Ta}$ ). For example, in  $\text{CsV}_3\text{Sb}_{5-x}\text{Sn}_x$ , the CDW correlation length along the  $H$  direction and  $L$  direction is 367 Å and 70 Å, respectively. The CDW correlation length along the  $H$  direction in  $\text{Cs}(\text{V}_{1-x}\text{Ta}_x)_3\text{Sb}_5$  ( $x = 0.067$ ) is reduced to 63 Å and 21 Å, respectively. Previous studies indicate that substitution of Sb primarily affects the Sb-derived electron-like band at the  $\Gamma$  point [25], whereas substitution of V by Nb enlarges the electron pocket at the  $\Gamma$  point and lifts the vHSs at the  $M$  point up and above Fermi level [15,29]. Therefore, the change of the electronic band at the  $M$  point degrades the nesting condition and suppresses the CDW. Additionally, substitution of V by Nb/Ta introduces disorder [38], which further suppresses the CDW phase by reducing CDW correlation length [39–41].

We then discuss the phase diagram of  $\text{Cs}(\text{V}_{1-x}\text{M}_x)_3\text{Sb}_5$  ( $M = \text{Nb}, \text{Ta}$ ) as shown in Fig. 1. While the CDW transition is rapidly suppressed with substitution, we observe that the increase in  $T_c$  becomes less efficient after the initial enhancement until the CDW phase is fully suppressed. Our XRD

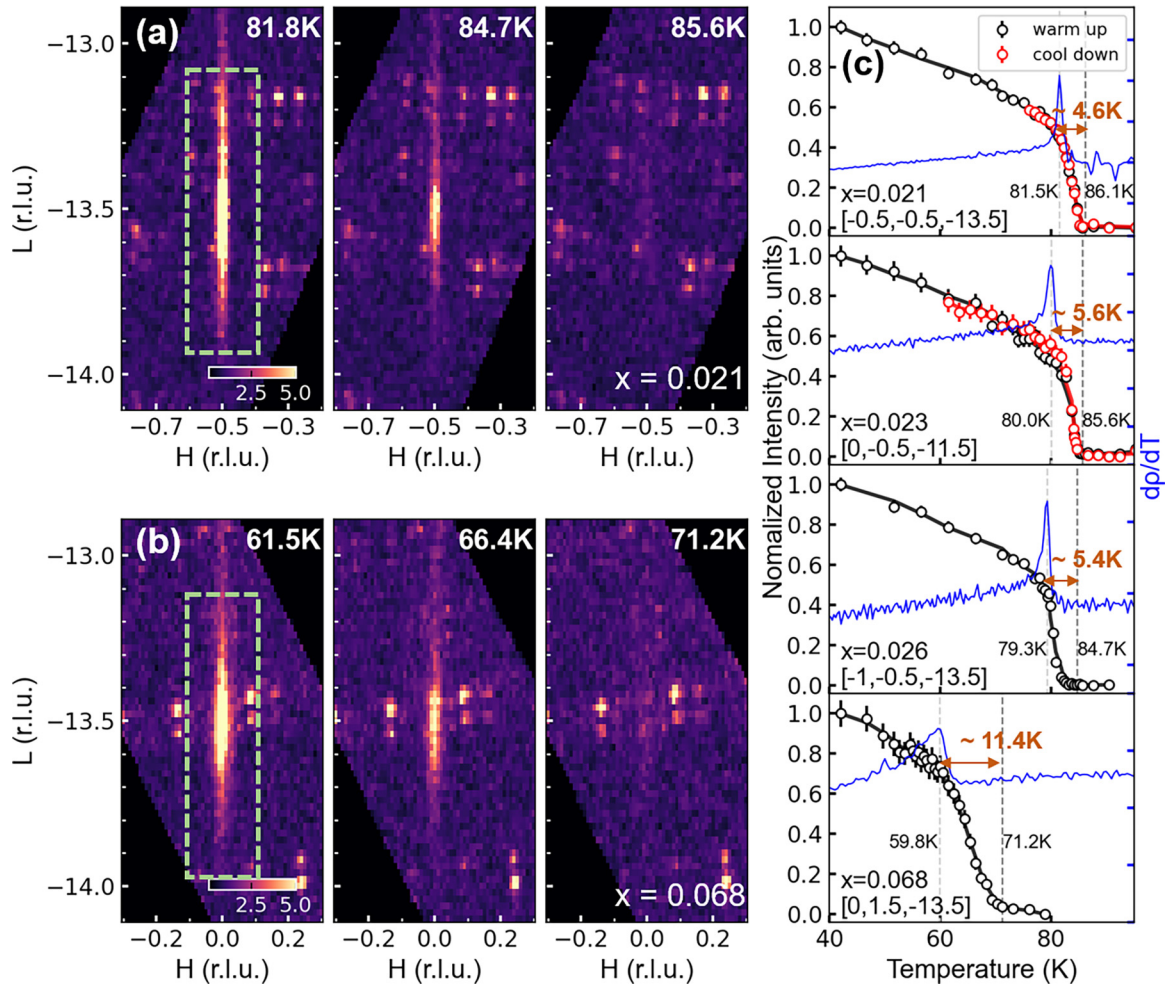


FIG. 6. Temperature dependence of the CDW in Nb-substituted samples. (a) The CDW profiles in  $x = 0.021$  measured at 81.8 K, 84.7 K, and 85.6 K. (b) The CDW profiles in  $x = 0.068$  measured at 61.5 K, 66.4 K, and 71.2 K. (c) Temperature dependence of CDW in four Nb-substituted samples. The transition temperature and the transition width are indicated in the figure. The temperature evolution curves also show good agreement during the warming and cooling processes. The  $d\rho/dT$  curve is also appended for comparison. The dashed lines indicate the onset decrease and disappearance of the CDW peak intensity. The transition width is indicated in the figure.

results demonstrate that substituting V by Ta/Nb causes the  $2 \times 2 \times 4$  CDW phase in  $\text{CsV}_3\text{Sb}_5$  to disappear. Given the absence of the  $2 \times 2 \times 4$  CDW phase [22,42,43] and that the unusual relationship between CDW and superconductivity is absent in  $\text{KV}_3\text{Sb}_5$  and  $\text{RbV}_3\text{Sb}_5$  [23–27], we speculate that the initial increase in  $T_c$  is attributed to the destruction of the  $2 \times 2 \times 4$  CDW phase. This is because CDW and superconductivity compete for the same density of states near the Fermi level [29,44,45]. Subsequently,  $T_c$  remains almost unchanged as the Ta/Nb substitution level increases, possibly due to a complicated interplay among  $2 \times 2 \times 2$  CDW, electronic nematicity [20,46], and superconductivity. Only upon the complete disappearance of the CDW phase do we observe a second enhancement of  $T_c$ .

We would like to note that we did not observe incommensurate quasi-1D electron correlations in  $\text{Cs}(\text{V}_{1-x}\text{M}_x)_3\text{Sb}_5$  ( $M = \text{Nb}, \text{Ta}$ ), as found in  $\text{CsV}_3\text{Sb}_{5-x}\text{Sn}_x$  [30]. This difference could be related to the distinct phase diagrams of the two systems. In  $\text{CsV}_3\text{Sb}_{5-x}\text{Sn}_x$ , incommensurate quasi-1D electron correlations were observed in the region between the double peaks of  $T_c$ . Similarly, a stripelike CDW order

was revealed by nuclear magnetic resonance measurements in pressurized  $\text{CsV}_3\text{Sb}_5$  [47]. This stripe order is argued to be responsible for the suppression of  $T_c$  between double peaks [47], where the superconducting transition is broad [23,24]. However, the superconducting transition is sharp in both Sn-doped and Ta/Nb-substituted  $\text{CsV}_3\text{Sb}_5$  samples. On the other hand, the incommensurate quasi-1D electron correlations observed in  $\text{CsV}_3\text{Sb}_{5-x}\text{Sn}_x$  are likely related to the distribution of Sb atoms, which have been shown to be involved in CDW formation through resonant x-ray scattering study on  $\text{CsV}_3\text{Sb}_5$  [48]. The doping of Sb with Sn may prompt the emergence of quasi-1D electron correlations by inducing a reconstruction of Fermi pockets [49].

We also notice that the phase diagram of  $\text{Cs}(\text{V}_{1-x}\text{M}_x)_3\text{Sb}_5$  ( $M = \text{Nb}, \text{Ta}$ ) is different from that of  $\text{Cs}(\text{V}_{1-x}\text{Ti}_x)_3\text{Sb}_5$ . There have been no reports of two distinct superconducting domes in  $\text{Cs}(\text{V}_{1-x}\text{M}_x)_3\text{Sb}_5$  ( $M = \text{Nb}, \text{Ta}$ ), even with substituting levels up to the solubility limit [28]. In contrast, hole-doped  $\text{Cs}(\text{V}_{1-x}\text{Ti}_x)_3\text{Sb}_5$  exhibit two types of superconducting domes, with the second dome emerging after the disappearance of the CDW order. The difference may

be related to different gap symmetries in CsV<sub>3</sub>Sb<sub>5</sub>-derived systems. Recent angle-resolved photoemission spectroscopy studies on Cs(V<sub>1-x</sub>Ta<sub>x</sub>)<sub>3</sub>Sb<sub>5</sub> and Cs(V<sub>1-x</sub>Nb<sub>x</sub>)<sub>3</sub>Sb<sub>5</sub> found the nodeless and isotropic superconducting gap is robust against the presence or absence of CDW [28]. In hole-doped Cs(V<sub>1-x</sub>Ti<sub>x</sub>)<sub>3</sub>Sb<sub>5</sub>, however, an unconventional V-shape superconductivity gap coexists with CDW at the low doping level, while it becomes U-shaped concomitant with the absence of CDW at high doping levels [14]. Furthermore,  $T_c$  monotonically decreases with increasing Ti doping level in the first dome [14,50]. This is because Ti substitution introduces holes into the system, which is different from the isovalent substitution of V atoms with Ta/Nb. This leads to the shrinking of the electron pocket at the  $\Gamma$  point [14], which is responsible for superconductivity [15,25,29], resulting in the decrease of  $T_c$  with Ti doping.

## V. CONCLUSIONS

In summary, our comprehensive x-ray diffraction experiments reveal the evolution of CDW in Cs(V<sub>1-x</sub>M<sub>x</sub>)<sub>3</sub>Sb<sub>5</sub> ( $M = \text{Nb, Ta}$ ). Our results show that the long-range three-dimensional  $2 \times 2 \times 4$  and  $2 \times 2 \times 2$  CDW phases coexisting in the pristine crystal evolve into a short-range quasi-two-dimensional  $2 \times 2 \times 2$  CDW phase upon substituting V with Ta/Nb. We confirm that the  $2 \times 2 \times 4$  CDW phase is rapidly destroyed by even a slight substitution, as evidenced by the absence of hysteresis behavior in the substituted samples. The CDW correlation lengths in both in-plane and out-of-plane directions are reduced upon substitution. Specifically,

in the Cs(V<sub>1-x</sub>Ta<sub>x</sub>)<sub>3</sub>Sb<sub>5</sub> ( $x = 0.067$ ) sample, the correlation lengths along the  $H$  and  $K$  directions are reduced to 63 Å and 87 Å, respectively, while the correlation length along the out-of-plane direction is reduced to 21 Å ( $\sim 2c$ ), indicating a two-dimensional CDW nature. Our experiments also show that we did not observe quasi-1D electron correlations in Cs(V<sub>1-x</sub>M<sub>x</sub>)<sub>3</sub>Sb<sub>5</sub> ( $M = \text{Nb, Ta}$ ) as those found in CsV<sub>3</sub>Sb<sub>5-x</sub>Sn<sub>x</sub> [30], which demonstrates that substituting V sites is different from doping Sb sites in CsV<sub>3</sub>Sb<sub>5</sub>. Our results, therefore, uncover the evolution of CDW with isovalent substitution of V sites in CsV<sub>3</sub>Sb<sub>5</sub>-derived materials and provide new insights into the underlying connections between CDW and superconductivity.

## ACKNOWLEDGMENTS

Y.Y.P. is grateful for financial support from the Ministry of Science and Technology of China (Grants No. 2019YFA0308401 and No. 2021YFA1401903) and the National Natural Science Foundation of China (Grant No. 11974029). Z.W. acknowledges the financial support from the National Key Research and Development Program of China (Grants No. 2020YFA0308800 and No. 2022YFA1403400), the National Science Foundation of China (NSFC) (Grant No. 92065109), and Beijing Natural Science Foundation (Grants No. Z210006 and No. Z190006). Z.W. thanks the Analysis and Testing Center at BIT for assistance in facility support. We thank Y. G. Yao for the support during the initial stage of the research. Y.F.G. acknowledges the financial support from the National Science Foundation of China (Grant No. 92065201).

- 
- [1] S. Yan, D. A. Huse, and S. R. White, Spin-liquid ground state of the  $S = 1/2$  kagome Heisenberg antiferromagnet, *Science* **332**, 1173 (2011).
  - [2] M. R. Norman, Colloquium: Herbertsmithite and the search for the quantum spin liquid, *Rev. Mod. Phys.* **88**, 041002 (2016).
  - [3] Y. Zhou, K. Kanoda, and T.-K. Ng, Quantum spin liquid states, *Rev. Mod. Phys.* **89**, 025003 (2017).
  - [4] S.-L. Yu and J.-X. Li, Chiral superconducting phase and chiral spin-density-wave phase in a Hubbard model on the kagome lattice, *Phys. Rev. B* **85**, 144402 (2012).
  - [5] M. L. Kiesel, C. Platt, and R. Thomale, Unconventional Fermi Surface Instabilities in the Kagome Hubbard Model, *Phys. Rev. Lett.* **110**, 126405 (2013).
  - [6] W.-S. Wang, Z.-Z. Li, Y.-Y. Xiang, and Q.-H. Wang, Competing electronic orders on kagome lattices at van Hove filling, *Phys. Rev. B* **87**, 115135 (2013).
  - [7] B. R. Ortiz, S. M. L. Teicher, Y. Hu, J. L. Zuo, P. M. Sarte, E. C. Schueller, A. M. M. Abeykoon, M. J. Krogstad, S. Rosenkranz, R. Osborn *et al.*, CsV<sub>3</sub>Sb<sub>5</sub>: A  $\mathbb{Z}_2$  Topological Kagome Metal with a Superconducting Ground State, *Phys. Rev. Lett.* **125**, 247002 (2020).
  - [8] B. R. Ortiz, P. M. Sarte, E. M. Kenney, M. J. Graf, S. M. L. Teicher, R. Seshadri, and S. D. Wilson, Superconductivity in the  $\mathbb{Z}_2$  kagome metal KV<sub>3</sub>Sb<sub>5</sub>, *Phys. Rev. Mater.* **5**, 034801 (2021).
  - [9] Q. Yin, Z. Tu, C. Gong, Y. Fu, S. Yan, and H. Lei, Superconductivity and normal-state properties of kagome metal RbV<sub>3</sub>Sb<sub>5</sub> single crystals, *Chin. Phys. Lett.* **38**, 037403 (2021).
  - [10] Y.-X. Jiang, J.-X. Yin, M. M. Denner, N. Shumiya, B. R. Ortiz, G. Xu, Z. Guguchia, J. He, M. S. Hossain, X. Liu *et al.*, Unconventional chiral charge order in kagome superconductor KV<sub>3</sub>Sb<sub>5</sub>, *Nat. Mater.* **20**, 1353 (2021).
  - [11] S.-Y. Yang, Y. Wang, B. Ortiz, D. Liu, J. Gayles, E. Derunova, R. Gonzalez-Hernandez, L. Šmejkal, Y. Chen, S. Parkin *et al.*, Giant, unconventional anomalous Hall effect in the metallic frustrated magnet candidate, KV<sub>3</sub>Sb<sub>5</sub>, *Sci. Adv.* **6**, eabb6003 (2020).
  - [12] F. H. Yu, T. Wu, Z. Y. Wang, B. Lei, W. Z. Zhuo, J. J. Ying, and X. H. Chen, Concurrence of anomalous Hall effect and charge density wave in a superconducting topological kagome metal, *Phys. Rev. B* **104**, L041103 (2021).
  - [13] E. M. Kenney, B. R. Ortiz, C. Wang, S. D. Wilson, and M. J. Graf, Absence of local moments in the kagome metal KV<sub>3</sub>Sb<sub>5</sub> as determined by muon spin spectroscopy, *J. Phys.: Condens. Matter* **33**, 235801 (2021).
  - [14] H. Yang, Z. Huang, Y. Zhang, Z. Zhao, J. Shi, H. Luo, L. Zhao, G. Qian, H. Tan, B. Hu *et al.*, Titanium doped kagome superconductor CsV<sub>3-x</sub>Ti<sub>x</sub>Sb<sub>5</sub> and two distinct phases, *Sci. Bull.* **67**, 2176 (2022).
  - [15] Y. Li, Q. Li, X. Fan, J. Liu, Q. Feng, M. Liu, C. Wang, J.-X. Yin, J. Duan, X. Li *et al.*, Tuning the competition between superconductivity and charge order in the kagome superconductor Cs(V<sub>1-x</sub>Nb<sub>x</sub>)<sub>3</sub>Sb<sub>5</sub>, *Phys. Rev. B* **105**, L180507 (2022).
  - [16] Q. Wu, Z. X. Wang, Q. M. Liu, R. S. Li, S. X. Xu, Q. W. Yin, C. S. Gong, Z. J. Tu, H. C. Lei, T. Dong *et al.*, Simultaneous

- formation of twofold rotation symmetry with charge order in the kagome superconductor  $\text{CsV}_3\text{Sb}_5$  by optical polarization rotation measurement, *Phys. Rev. B* **106**, 205109 (2022).
- [17] Y. Xu, Z. Ni, Y. Liu, B. R. Ortiz, Q. Deng, S. D. Wilson, B. Yan, L. Balents, and L. Wu, Three-state nematicity and magneto-optical Kerr effect in the charge density waves in kagome superconductors, *Nat. Phys.* **18**, 1470 (2022).
- [18] H. Li, H. Zhao, B. R. Ortiz, T. Park, M. Ye, L. Balents, Z. Wang, S. D. Wilson, and I. Zeljkovic, Rotation symmetry breaking in the normal state of a kagome superconductor  $\text{KV}_3\text{Sb}_5$ , *Nat. Phys.* **18**, 265 (2022).
- [19] Y. Xiang, Q. Li, Y. Li, W. Xie, H. Yang, Z. Wang, Y. Yao, and H.-H. Wen, Twofold symmetry of  $c$ -axis resistivity in topological kagome superconductor  $\text{CsV}_3\text{Sb}_5$  with in-plane rotating magnetic field, *Nat. Commun.* **12**, 6727 (2021).
- [20] L. Nie, K. Sun, W. Ma, D. Song, L. Zheng, Z. Liang, P. Wu, F. Yu, J. Li, M. Shan *et al.*, Charge-density-wave-driven electronic nematicity in a kagome superconductor, *Nature (London)* **604**, 59 (2022).
- [21] C. Mielke, D. Das, J. X. Yin, H. Liu, R. Gupta, Y. X. Jiang, M. Medarde, X. Wu, H. C. Lei, J. Chang *et al.*, Time-reversal symmetry-breaking charge order in a kagome superconductor, *Nature (London)* **602**, 245 (2022).
- [22] Q. Xiao, Y. Lin, Q. Li, X. Zheng, S. Francoual, C. Plueckthun, W. Xia, Q. Qiu, S. Zhang, Y. Guo *et al.*, Coexistence of multiple stacking charge density waves in kagome superconductor  $\text{CsV}_3\text{Sb}_5$ , *Phys. Rev. Res.* **5**, L012032 (2023).
- [23] F. H. Yu, D. H. Ma, W. Z. Zhuo, S. Q. Liu, X. K. Wen, B. Lei, J. J. Ying, and X. H. Chen, Unusual competition of superconductivity and charge-density-wave state in a compressed topological kagome metal, *Nat. Commun.* **12**, 3645 (2021).
- [24] K. Y. Chen, N. N. Wang, Q. W. Yin, Y. H. Gu, K. Jiang, Z. J. Tu, C. S. Gong, Y. Uwatoko, J. P. Sun, H. C. Lei *et al.*, Double Superconducting Dome and Triple Enhancement of  $T_c$  in the Kagome Superconductor  $\text{CsV}_3\text{Sb}_5$  under High Pressure, *Phys. Rev. Lett.* **126**, 247001 (2021).
- [25] Y. M. Oey, B. R. Ortiz, F. Kaboudvand, J. Frassinetti, E. Garcia, R. Cong, S. Sanna, V. F. Mitrović, R. Seshadri, and S. D. Wilson, Fermi level tuning and double-dome superconductivity in the kagome metal  $\text{CsV}_3\text{Sb}_{5-x}\text{Sn}_x$ , *Phys. Rev. Mater.* **6**, L041801 (2022).
- [26] Y. M. Oey, F. Kaboudvand, B. R. Ortiz, R. Seshadri, and S. D. Wilson, Tuning charge density wave order and superconductivity in the kagome metals  $\text{KV}_3\text{Sb}_{5-x}\text{Sn}_x$  and  $\text{RbV}_3\text{Sb}_{5-x}\text{Sn}_x$ , *Phys. Rev. Mater.* **6**, 074802 (2022).
- [27] T. Neupert, M. M. Denner, J.-X. Yin, R. Thomale, and M. Z. Hasan, Charge order and superconductivity in kagome materials, *Nat. Phys.* **18**, 137 (2022).
- [28] Y. Zhong, J. Liu, X. Wu, Z. Guguchia, J.-X. Yin, A. Mine, Y. Li, S. Najafzadeh, D. Das, C. M. III *et al.*, Nodeless electron pairing in  $\text{CsV}_3\text{Sb}_5$ -derived kagome superconductors, *Nature (London)* **617**, 488 (2023).
- [29] T. Kato, Y. Li, K. Nakayama, Z. Wang, S. Souma, F. Matsui, M. Kitamura, K. Horiba, H. Kumigashira, T. Takahashi *et al.*, Fermiology and Origin of  $T_c$  Enhancement in a Kagome Superconductor  $\text{Cs}(\text{V}_{1-x}\text{Nb}_x)_3\text{Sb}_5$ , *Phys. Rev. Lett.* **129**, 206402 (2022).
- [30] L. Kautzsch, Y. M. Oey, H. Li, Z. Ren, B. R. Ortiz, R. Seshadri, J. Ruff, Z. Wang, I. Zeljkovic, and S. D. Wilson, Incommensurate charge-stripe correlations in the kagome superconductor  $\text{CsV}_3\text{Sb}_{5-x}\text{Sn}_x$ , [arXiv:2207.10608](https://arxiv.org/abs/2207.10608).
- [31] H. Tan, Y. Liu, Z. Wang, and B. Yan, Charge Density Waves and Electronic Properties of Superconducting Kagome Metals, *Phys. Rev. Lett.* **127**, 046401 (2021).
- [32] Y. Xie, Y. Li, P. Bourges, A. Ivanov, Z. Ye, J.-X. Yin, M. Z. Hasan, A. Luo, Y. Yao, Z. Wang *et al.*, Electron-phonon coupling in the charge density wave state of  $\text{CsV}_3\text{Sb}_5$ , *Phys. Rev. B* **105**, L140501 (2022).
- [33] G. Liu, X. Ma, K. He, Q. Li, H. Tan, Y. Liu, J. Xu, W. Tang, K. Watanabe, T. Taniguchi *et al.*, Observation of anomalous amplitude modes in the kagome metal  $\text{CsV}_3\text{Sb}_5$ , *Nat. Commun.* **13**, 3461 (2022).
- [34] J.-G. Si, W.-J. Lu, Y.-P. Sun, P.-F. Liu, and B.-T. Wang, Charge density wave and pressure-dependent superconductivity in the kagome metal  $\text{CsV}_3\text{Sb}_5$ : A first-principles study, *Phys. Rev. B* **105**, 024517 (2022).
- [35] K. Fukushima, K. Obata, S. Yamane, Y. Hu, Y. Li, Y. Yao, Z. Wang, Y. Maeno, and S. Yonezawa, Violation of emergent rotational symmetry in the hexagonal kagome superconductor  $\text{CsV}_3\text{Sb}_5$ , [arXiv:2303.11072](https://arxiv.org/abs/2303.11072).
- [36] J. Li, W. Xie, J. Liu, Q. Li, X. Li, H. Yang, Z. Wang, Y. Yao, and H.-H. Wen, Strong-coupling superconductivity and weak vortex pinning in Ta-doped  $\text{CsV}_3\text{Sb}_5$  single crystals, *Phys. Rev. B* **106**, 214529 (2022).
- [37] L. D. Sanjeewa, Y. Liu, J. Xing, R. S. Fishman, M. T. K. Kolambage, M. A. McGuire, C. D. McMillen, J. W. Kolis, and A. S. Sefat, Stacking faults and short-range magnetic correlations in single crystal  $\text{Y}_3\text{Ru}_2\text{O}_{12}$ : A structure with  $\text{Ru}^{+4.5}$  one-dimensional chains, *Phys. Status Solidi B* **258**, 2000197 (2021).
- [38] X. Zhou, Y. Li, Z. Liu, J. Hao, Y. Dai, Z. Wang, Y. Yao, and H.-H. Wen, Effects of niobium doping on the charge density wave and electronic correlations in the kagome metal  $\text{Cs}(\text{V}_{1-x}\text{Nb}_x)_3\text{Sb}_5$ , *Phys. Rev. B* **107**, 125124 (2023).
- [39] M. Leroux, V. Mishra, J. P. C. Ruff, H. Claus, M. P. Smylie, C. Opagiste, P. Rodière, A. Kayani, G. D. Gu, J. M. Tranquada *et al.*, Disorder raises the critical temperature of a cuprate superconductor, *Proc. Natl. Acad. Sci. USA* **116**, 10691 (2019).
- [40] L. Li, X. Deng, Z. Wang, Y. Liu, M. Abeykoon, E. Dooryhee, A. Tomic, Y. Huang, J. B. Warren, E. S. Bozin *et al.*, Superconducting order from disorder in  $2H\text{-TaSe}_{2-x}\text{S}_x$ , *npj Quantum Mater.* **2**, 11 (2017).
- [41] H. Mutka, Superconductivity in irradiated charge-density-wave compounds  $2H\text{-NbSe}_2$ ,  $2H\text{-TaS}_2$ , and  $2H\text{-TaSe}_2$ , *Phys. Rev. B* **28**, 2855 (1983).
- [42] B. R. Ortiz, S. M. L. Teicher, L. Kautzsch, P. M. Sarte, N. Ratcliff, J. Harter, J. P. C. Ruff, R. Seshadri, and S. D. Wilson, Fermi Surface Mapping and the Nature of Charge-Density-Wave Order in the Kagome Superconductor  $\text{CsV}_3\text{Sb}_5$ , *Phys. Rev. X* **11**, 041030 (2021).
- [43] L. Kautzsch, B. R. Ortiz, K. Mallayya, J. Plumb, G. Pokharel, J. P. C. Ruff, Z. Islam, E.-A. Kim, R. Seshadri, and S. D. Wilson, Structural evolution of the kagome superconductors  $\text{AV}_3\text{Sb}_5$  ( $A = \text{K}, \text{Rb}, \text{and Cs}$ ) through charge density wave order, *Phys. Rev. Mater.* **7**, 024806 (2023).
- [44] H.-S. Xu, Y.-J. Yan, R. Yin, W. Xia, S. Fang, Z. Chen, Y. Li, W. Yang, Y. Guo, and D.-L. Feng, Multiband Superconductivity with Sign-Preserving Order Parameter in Kagome Superconductor  $\text{CsV}_3\text{Sb}_5$ , *Phys. Rev. Lett.* **127**, 187004 (2021).

- [45] T. Qian, M. H. Christensen, C. Hu, A. Saha, B. M. Andersen, R. M. Fernandes, T. Birol, and N. Ni, Revealing the competition between charge density wave and superconductivity in  $\text{CsV}_3\text{Sb}_5$  through uniaxial strain, *Phys. Rev. B* **104**, 144506 (2021).
- [46] P. Wu, Y. Tu, Z. Wang, S. Yu, H. Li, W. Ma, Z. Liang, Y. Zhang, X. Zhang, Z. Li *et al.*, Unidirectional electron-phonon coupling in the nematic state of a kagome superconductor, *Nat. Phys.* (2023), doi: [10.1038/s41567-023-02031-5](https://doi.org/10.1038/s41567-023-02031-5).
- [47] L. Zheng, Z. Wu, Y. Yang, L. Nie, M. Shan, K. Sun, D. Song, F. Yu, J. Li, D. Zhao *et al.*, Emergent charge order in pressurized kagome superconductor  $\text{CsV}_3\text{Sb}_5$ , *Nature (London)* **611**, 682 (2022).
- [48] H. Li, G. Fabbris, A. H. Said, J. P. Sun, Y.-X. Jiang, J. X. Yin, Y.-Y. Pai, S. Yoon, A. R. Lupini, C. S. Nelson *et al.*, Discovery of conjoined charge density waves in the kagome superconductor  $\text{CsV}_3\text{Sb}_5$ , *Nat. Commun.* **13**, 6348 (2022).
- [49] H. Li, D. Oh, M. Kang, H. Zhao, B. R. Ortiz, Y. Oey, S. Fang, Z. Ren, C. Jozwiak, A. Bostwick *et al.*, Small Fermi pockets intertwined with charge stripes and pair density wave order in a kagome superconductor, [arXiv:2303.07254](https://arxiv.org/abs/2303.07254).
- [50] Y. Liu, Y. Wang, Y. Cai, Z. Hao, X.-M. Ma, L. Wang, C. Liu, J. Chen, L. Zhou, J. Wang *et al.*, Doping evolution of superconductivity, charge order, and band topology in hole-doped topological kagome superconductors  $\text{Cs}(\text{V}_{1-x}\text{Ti}_x)_3\text{Sb}_5$ , *Phys. Rev. Mater.* **7**, 064801 (2023).